

SUPPLEMENTARY MATERIALS: A KINETIC MONTE CARLO APPROACH FOR SIMULATING CASCADING TRANSMISSION LINE FAILURE*

JACOB ROTH[†], DAVID A. BARAJAS-SOLANO[‡], PANOS STINIS[‡], JONATHAN WEARE[§], AND MIHAI ANITESCU[†]

SM1. Port-Hamiltonian power transmission model and energy function. For the following presentation of the stochastic dynamics model (2.7)* we will employ the following notation: For vector quantities in \mathbb{R}^N or \mathbb{C}^N , we denote by $[\cdot]_X$ the subvector corresponding to the subset of indices $X \subseteq [1, N]$. For square matrices of dimension N , we denote by $[\cdot]_X$ the diagonal block corresponding to the subset $X \subseteq [1, N]$ of row and column indices. Next, we denote the identity matrix of dimension $|X|$ by \mathbb{I}_X , the vector of ones of dimension $|X|$ by $\mathbf{1}_X$, and rectangular zero matrices of $|X|$ rows and $|Y|$ columns by $\mathbf{0}_{X \times Y}$. Finally, we denote by \odot the Hadamard product.

AC power flow equations. The state of the i th bus at time t is specified by its net power phasor, $[S_t]_i := [P_t]_i + j[Q_t]_i$, and its voltage phasor, $[v_t]_i := [V_t]_i \exp(j[\delta_t]_i)$, where $[P_t]_i$ and $[Q_t]_i$ denote the net active and reactive powers, respectively, j denotes the imaginary unit, and $[V_t]_i$ and $[\delta_t]_i$ denote the voltage magnitude and phase angle, respectively. The power and voltage phasors are related via the AC power flow equations

$$[S_t]_i = [v_t \odot (Y v_t)^*]_i, \quad i \in \mathcal{B}$$

where the complex matrix $Y := G + jB$ denotes the network admittance matrix. Assuming that the network is lossless, we have that Y is purely imaginary, with $Y = jB$. The real and imaginary components of the AC power flow equations read

$$(SM1.1a) \quad [P_t]_i = \sum_{k \in \mathcal{B}} [V_t]_i [V_t]_k B_{ik} \sin ([\delta_t]_i - [\delta_t]_k),$$

$$(SM1.1b) \quad [Q_t]_i = - \sum_{k \in \mathcal{B}} [V_t]_i [V_t]_k B_{ik} \cos ([\delta_t]_i - [\delta_t]_k), \quad i \in \mathcal{B}.$$

Here, we adopt the convention that $[P_t]_i := [P_t^g]_i - [P_t^d]_i$ and $[Q_t]_i := [Q_t^d]_i - [Q_t^g]_i$. Hence, $[P_t]_i > 0$ ($[Q_t]_i > 0$) indicates that net active (reactive) power is being injected at the i th bus, while $[P_t]_i < 0$ ($[Q_t]_i < 0$) indicates that net active (reactive) power is being consumed at the i th bus.

We assume that at $t = 0$ the system is at equilibrium and the generators are synchronized. Generator buses are modeled as PV buses, so that their equilibrium values of net real power and voltage magnitudes, $[P_0]_{\mathcal{G}}$ and $[V_0]_{\mathcal{G}}$, respectively, are prescribed. For the reference bus, on the other

*Supplementary material for MMS MS#M130686.

<https://doi.org/10.1137/19M1306865>

[†]Mathematics and Computer Science Division, Argonne National Laboratory, Lemont, IL, 60439 (jm-roth@mcs.anl.gov, anitescu@mcs.anl.gov).

[‡]Pacific Northwest National Laboratory, Richland, WA, 99354 (David.Barajas-Solano@pnnl.gov, panos.stinis@pnnl.gov).

[§]Courant Institute of Mathematical Sciences, New York University, New York, NY, 10012-1185 (weare@cims.nyu.edu).

*The presentation of the deterministic component of the model closely follows the references [SM7, SM8], and the presentation of the stochastic component of the model closely follows [SM2] (but does not include excitation voltage perturbations since the models in [SM7, SM8] do not include flux-decay dynamics).

hand, the voltage magnitude and angle, $[V_0]_{\mathcal{S}}$ and $[\delta_0]_{\mathcal{S}}$, are specified. Finally, for load buses, the equilibrium values of the net real and reactive powers, $[P_0]_{\mathcal{L}}$ and $[Q_0]_{\mathcal{L}}$, respectively, are prescribed. The AC power flow equations (SM1.1a) and (SM1.1b) can be solved together with these prescribed quantities to calculate all other equilibrium quantities.

Classical machine model. Generators are modeled using the classical model. The deterministic dynamics of the generators are then governed by the swing equations

$$(SM1.2a) \quad [M^g]_{ii}[\dot{\omega}_t]_i = -[D^g]_{ii}[\omega_t]_i - [P_t]_i + [P_0]_i,$$

$$(SM1.2b) \quad [\dot{\delta}_t]_i = [\omega_t]_i, \quad i \in \mathcal{S} \cup \mathcal{G},$$

where $[\omega_t]_i$ denotes the generator angular velocity of the i th bus, and M^g and D^g denote the diagonal matrices of generator mass and damping constants.

For generator buses we assume that their voltage magnitudes remain constant throughout the evolution of the system, so that $[V_t]_{\mathcal{G}} \equiv [V_0]_{\mathcal{G}}$. Introducing the auxiliary angular variables

$$(SM1.3) \quad [\theta_t]_i := [\delta_t]_i - [\delta_0]_{\mathcal{S}}, \quad i \in \mathcal{G} \cup \mathcal{L},$$

we can rewrite the AC power flow equations (SM1.1a) and (SM1.1b) for $i \in \mathcal{G} \cup \mathcal{L}$ in terms of the auxiliary functions f_i and g_i defined as

$$(SM1.4a)$$

$$[P_t]_i = f_i([\theta_t]_{\mathcal{G} \cup \mathcal{L}}, [V_t]_{\mathcal{L}}) := \sum_{k \in \mathcal{G} \cup \mathcal{L}} [V_t]_i [V_t]_k B_{ik} \sin ([\theta_t]_i - [\theta_t]_k) + B_{iS} [V_t]_i [V_t]_S \sin ([\theta_t]_i),$$

$$(SM1.4b)$$

$$[Q_t]_i = g_i([\theta_t]_{\mathcal{G} \cup \mathcal{L}}, [V_t]_{\mathcal{L}}) := - \sum_{k \in \mathcal{G} \cup \mathcal{L}} [V_t]_k [V_t]_i B_{ik} \cos ([\theta_t]_i - [\theta_t]_k) - B_{iS} [V_t]_i [V_t]_S \cos ([\theta_t]_i), \\ i \in \mathcal{G} \cup \mathcal{L}.$$

Finally, we note that (i) as the system is lossless, the net real power at all buses is zero and (ii) by setting a reference angle, we have the implicit constraint $\sum_j \theta_j = 0$. From this, it follows that

$$[P_t]_{\mathcal{S}} - [P_0]_{\mathcal{S}} = - \sum_{i \in \mathcal{G} \cup \mathcal{L}} \{[f]_i - [P_0]_i\}.$$

We can then rewrite the swing equations (SM1.2a) and (SM1.2b) as

$$(SM1.5a) \quad [M^g]_{\mathcal{S}}[\dot{\omega}_t]_{\mathcal{S}} = -[D^g]_{\mathcal{S}}[\omega_t]_{\mathcal{S}} + \sum_{i \in \mathcal{G} \cup \mathcal{L}} \{[f]_i - [P_0]_i\},$$

$$(SM1.5b) \quad [M^g]_{\mathcal{G}}[\dot{\omega}_t]_{\mathcal{G}} = -[D^g]_{\mathcal{G}}[\omega_t]_{\mathcal{G}} - [f]_{\mathcal{G}} + [P_0]_{\mathcal{G}},$$

$$(SM1.5c) \quad [\dot{\theta}_t]_{\mathcal{G}} = -\mathbf{1}_{\mathcal{G}}[\omega_t]_{\mathcal{S}} + [\omega_t]_{\mathcal{G}}.$$

Deterministic load model. For load buses, we model the real power as linear functions of the bus angular velocity, and we assume that the reactive power remains constant throughout the simulation:

$$(SM1.6a) \quad [P_t]_i := [P_0]_i - [D^d]_{ii}[\dot{\delta}_t]_i,$$

$$(SM1.6b) \quad [Q_t]_i := [Q_0]_i, \quad i \in \mathcal{L}.$$

where D^d is a diagonal matrix of load damping constants. In terms of the relative phase angles θ , (SM1.6a) can be rewritten as

$$(SM1.7) \quad [\dot{\theta}_t]_{\mathcal{L}} = -[D^d]_{\mathcal{L}}^{-1} \{ [f]_{\mathcal{L}} - [P_0]_{\mathcal{L}} \} - [\dot{\omega}_t]_{\mathcal{S}}.$$

DAE system. From (SM1.4a)–(SM1.7) it can be seen that the dynamics of the network can be described by $[\omega_t]_{\mathcal{S} \cup \mathcal{G}}$, $[\theta_t]_{\mathcal{G}}$, and $[V_t]_{\mathcal{L}}$. We collect these state variables into the state vector $x_t^\top := ([\omega_t]_{\mathcal{S} \cup \mathcal{G}}^\top, [\theta_t]_{\mathcal{G}}^\top, [V_t]_{\mathcal{L}}^\top)$. To assemble a system of DAEs governing the dynamics of x_t , we introduce the auxiliary functions

$$(SM1.8a) \quad H_1(x_t) := M^g[\omega_t]_{\mathcal{S} \cup \mathcal{G}},$$

$$(SM1.8b) \quad H_2(x_t) := [f(x_t)]_{\mathcal{G} \cup \mathcal{L}} - [P_0]_{\mathcal{G} \cup \mathcal{L}}.$$

and the matrices

$$T_1 = \begin{bmatrix} -\mathbb{1}_{\mathcal{G}} & \mathbb{I}_{\mathcal{G}} \\ -\mathbb{1}_{\mathcal{L}} & \mathbb{O}_{\mathcal{L} \times \mathcal{G}} \end{bmatrix}, \quad T_2 = \begin{bmatrix} \mathbb{O}_{\mathcal{G} \times \mathcal{L}} \\ \mathbb{I}_{\mathcal{L}} \end{bmatrix},$$

so that the governing equations (SM1.6b), (SM1.5) and (SM1.7) can be rewritten in DAE form as

$$(SM1.9a) \quad [\dot{\omega}_t]_{\mathcal{S} \cup \mathcal{G}} = -(M^g)^{-1} D^g (M^g)^{-1} H_1 - (M^g)^{-1} T_1^\top H_2,$$

$$(SM1.9b) \quad [\dot{\theta}_t]_{\mathcal{G} \cup \mathcal{L}} = T_1 (M^g)^{-1} H_1 - T_2 (D^d)^{-1} T_2^\top H_2,$$

$$(SM1.9c) \quad 0 = [V_t]_{\mathcal{L}}^{-1} \odot \{ [g]_{\mathcal{L}} - [Q_0]_{\mathcal{L}} \}$$

where the set of algebraic equations (SM1.9c) corresponds to the reactive load model (SM1.6b), which constrains the dynamics to the power flow manifold.

Singularly-perturbed ODE system. The DAE system (SM1.9) is not globally well posed. Following [SM2], we consider a singularly-perturbed version of the algebraic constraint with perturbation parameter D^ϵ such that in the limit $D^\epsilon \rightarrow 0^+$, the singularly-perturbed model approximates the DAE system arbitrarily well. Introducing the additional auxiliary function

$$(SM1.10) \quad H_3(x_t) := [V_t]_{\mathcal{L}}^{-1} \odot \{ [g]_{\mathcal{L}} - [Q_0]_{\mathcal{L}} \}$$

we can recast the DAE system (SM1.9) into the ODE system

$$(SM1.11a) \quad [\dot{\omega}_t]_{\mathcal{S} \cup \mathcal{G}} = -(M^g)^{-1} D^g (M^g)^{-1} H_1 - (M^g)^{-1} T_1^\top H_2,$$

$$(SM1.11b) \quad [\dot{\theta}_t]_{\mathcal{G} \cup \mathcal{L}} = T_1 (M^g)^{-1} H_1 - T_2 (D^d)^{-1} T_2^\top H_2,$$

$$(SM1.11c) \quad [\dot{V}_t]_{\mathcal{L}} = -(D^\epsilon)^{-1} H_3,$$

or in compact form,

$$(SM1.12) \quad \dot{x}_t = -KH(x_t),$$

where $H^\top := (H_1^\top, H_2^\top, H_3^\top)$, and $K := S - J$, with the matrices J and S given in the in the main article.

Energy function derivation. We proceed to obtain a candidate Lyapunov function. Defining $\nabla \mathcal{H}(x_t) := H(x_t)$, we can obtain $\mathcal{H}(x_t)$ by integrating $H(x)$ along a path from x_0 to x_t , that is,

$$(SM1.13) \quad \mathcal{H}(x_t) := \int_{(0, [\theta_0]_{\mathcal{G} \cup \mathcal{L}}, [V_0]_{\mathcal{L}})}^{([\omega_t]_{\mathcal{S} \cup \mathcal{G}}, [\theta_t]_{\mathcal{G} \cup \mathcal{L}}, [V_t]_{\mathcal{L}})} \langle H(y), dy \rangle.$$

Disregarding the constant of integration, we obtain the scalar potential [SM5, SM2, SM6, SM7, SM8]

$$\begin{aligned} \mathcal{H}(x_t) &= \frac{1}{2} [\omega_t]_{\mathcal{S} \cup \mathcal{G}}^\top M^g [\omega_t]_{\mathcal{S} \cup \mathcal{G}} + \frac{1}{2} \sum_{i,j \in \mathcal{B}} B_{ij} [V_t]_i [V_t]_j \cos([\theta_t]_i - [\theta_T]_j) \\ &\quad + \langle [P_0]_{\mathcal{G} \cup \mathcal{L}}, [\theta_t]_{\mathcal{G} \cup \mathcal{S}} \rangle + \langle [Q_0]_{\mathcal{L}}, \log([V_t]_{\mathcal{L}}) \rangle + C \\ &= \frac{1}{2} ([\omega_t]_{\mathcal{S} \cup \mathcal{G}})^\top M^g [\omega_t]_{\mathcal{S} \cup \mathcal{G}} + \frac{1}{2} v_t^\top B v_t + [P_0]_{\mathcal{G} \cup \mathcal{L}}^\top [\theta_t]_{\mathcal{G} \cup \mathcal{L}} + [Q_0]_{\mathcal{L}}^\top \log([V_t]_{\mathcal{L}}), \end{aligned}$$

thus recovering the energy function. Substituting this energy function into the ODE system (SM1.11) leads to the port-Hamiltonian form of the system dynamics. Also, it can be verified that the condition $\nabla \mathcal{H}(x) = 0$ is equivalent to the power flow equations (SM1.1). Finally, we note that the equilibrium position \bar{x} is asymptotically stable [SM1].

Noise model. Following DeMarco [SM2], we introduce scaled, additive noise to the deterministic dynamics (SM1.11) in such a way as to satisfy fluctuation-dissipation dynamics. Specifically, this means adding independent Wiener processes with covariance (diffusion) matrix $\sqrt{S/2}$. We can interpret the stochastic fluctuations as direct perturbations to the elements of active and reactive power with magnitude Z_t^P and Z_t^Q , respectively. Componentwise, we now make this relationship explicit by replacing P_0 with $P_0 + Z_t^P$ and Q_0 with $Q_0 + Z_t^Q$. We then determine the appropriate scaling coefficients of Z_t^P and Z_t^Q in terms of the components of S .

Consider the stochastic dynamics

$$\begin{aligned} \dot{\omega}_{\mathcal{S}} &= -(M^g)^{-1} D^g \omega_{\mathcal{S}} - \mathbb{1}_{\mathcal{G} \cup \mathcal{L}}^\top [f - (P_0 + Z_t^P)]_{\mathcal{G} \cup \mathcal{L}} \\ \dot{\omega}_{\mathcal{G}} &= -(M^g)^{-1} D^g \omega_{\mathcal{G}} + (M^g)^{-1} \mathbb{I}_{\mathcal{G}} [f - (P_0 + Z_t^P)]_{\mathcal{G}} \\ (SM1.14) \quad \dot{\theta}_{\mathcal{G}} &= -\mathbb{1}_{\mathcal{G}} \omega_{\mathcal{S}} - \omega_{\mathcal{G}} \\ \dot{\theta}_{\mathcal{L}} &= -\mathbb{1}_{\mathcal{L}} \omega_{\mathcal{S}} + (D^d)^{-1} [f - (P_0 + Z_t^P)]_{\mathcal{L}} \\ \dot{V}_{\mathcal{L}} &= V_{\mathcal{L}}^{-1} \odot [g - (Q_0 + Z_t^Q)]_{\mathcal{L}} \end{aligned}$$

and define

$$\begin{aligned} (SM1.15) \quad [Z_t^P]_i &:= (M^g)^{-1} D^g (M^g)^{-1} [\mathrm{d}W_t]_i, & i \in \mathcal{S} \\ [Z_t^P]_i &:= D^g (M^g)^{-1} [\mathrm{d}W_t]_i, & i \in \mathcal{G} \\ [Z_t^P]_i &:= [\mathrm{d}W_t]_i, & i \in \mathcal{L} \end{aligned}$$

and

$$\begin{aligned} (SM1.16) \quad [Z_t^Q]_i &:= 0, & i \in \mathcal{S} \\ [Z_t^Q]_i &:= 0, & i \in \mathcal{G} \\ [Z_t^Q]_i &:= V_{\mathcal{L}} [\mathrm{d}W_t]_i, & i \in \mathcal{L}. \end{aligned}$$

We remark that (SM1.14) yields the same dynamics as $-K\nabla\mathcal{H}(x) + \sqrt{2S}\mathrm{d}W_t$ if we assume that at the reference (slack) bus, the aggregate frequency dynamics are computed on power balance differences with respect to the unperturbed P_0 (following [SM2]) but are perturbed according to an independent forcing term with magnitude $(M^g)^{-1}D^g(M^g)^{-1}$. In [SM2], it is assumed that there is no additional independent forcing term; in our model, this amounts to removing damping from the generator equation. For consistency with the other generators, we include slack generator damping (and its corresponding scaled noise). Finally, we control the magnitude of the additive noise by τ . Thus, the noise model introduces stochastic disturbances to the (i) active power at both load and generator buses, and (ii) reactive power at the load buses.

SM2. Algorithm and data details. We provide additional detail on the KMC algorithm and data for a small test system.

SM2.1. Line limit calculation. For the adjusted DC method, current magnitude limits were set as the square root of DC limit data. DC limit data was computed through a system feedback loop where limits were iteratively increased if an overflow was observed in the network under OPA simulation (a cascading failure model developed at Oak Ridge National Laboratory used in [SM3]). The simulation was run 100 times until the network became reasonably stable and flow limits were such that failures were due to overloads due to initial failures rather than normal operating fluctuations. The DC limit data did not contain limits for each line, and we computed limits for the few remaining lines as the geometric average of the line's OPF flow and the maximum flow over all lines at the OPF point.

Algorithm SM2.1 Adjusted DC Approximation

```

Require: DC (real power) line limit data  $D$ , Network topology  $\mathcal{N}$ 
 $\hat{x}_0 \leftarrow \text{ACOPF}(\mathcal{N})$ 
 $\Theta_l = \Theta_l(\hat{x}_0)$ 
for  $l \in \mathcal{N}, \mathcal{L}$  do
    if  $l \in D$  then
         $\Theta_l^{\max} = \sqrt{D_l}$ 
    else
         $\Theta_l^{\max} = \sqrt{\max_k \{\Theta_k\} \times \Theta_l}$ 
    end if
end for
return  $\Theta^{\max}$ 

```

For the N -1 procedure, line limits were set to ensure N -1 feasibility under all non-islanding line failure contingencies (that is, line failures which do not separate a bus from the slack) in the heavily congested network settings. The method involves iteratively solving security-constrained AC optimal power flow problems (see [SM4]) at different loading levels.

Algorithm SM2.2 Loading-dependent N -1 Criteria

Require: Network \mathcal{N} , non-islanding contingencies \mathcal{C} , loading factor a , step factor b , power factor c , rating buffer d

```

while true do
     $\Theta^{\max} \leftarrow |Y_{ft}|^2 \times \left( (V_f^{\max})^2 + (V_t^{\max})^2 + 2V_f^{\max}V_t^{\max} \right) \forall (f, t) \in \mathcal{N} \cdot \mathcal{L}$  ▷ physically maximal current
    Adjust  $\mathcal{N}.P_d$  and  $\mathcal{N}.Q_d$  network data to  $a\%$  of generation total capacity, maintaining  $c$ 
     $\bar{x} \leftarrow \text{SC-ACOPF}(\mathcal{N}, \mathcal{C})$  ▷ run security constrained ACOPF
    for  $c \in \mathcal{C}$  do
         $\bar{x}_c \leftarrow \text{ACPF}(\mathcal{N}_c)$  ▷ run power flow to compute operating point  $\bar{x}_c$  under contingency  $c$ 
         $\Theta_c \leftarrow \Theta(\bar{x}_c)$  ▷ compute flows for the operating point  $\bar{x}_c$ 
    end for
     $\Theta^{\max} \leftarrow \max_c \Theta_c \times d$  ▷ update the vector of limits according to the maximum flow across contingencies
     $\bar{x} \leftarrow \text{SC-ACOPF}(\mathcal{N})$  for non-islanding line outages with new limits
    if  $\bar{x}$  is feasible (SC-ACOPF is solved optimally) then
        return  $\Theta^{\max}$ 
    else
         $a \leftarrow a - b$ 
    end if
end while

```

SM2.2. Markov model optimization routines. Occasionally, the Markov line failure computations may encounter either non-physical solutions or infeasibility. In these cases, as outlined in [Algorithm SM2.3](#), we remove all lines associated with bus- i , shed any load at bus i , and re-solve for a new equilibrium point until the resulting point \bar{x} has voltages that exceed 0.1 p.u. Similarly, the constrained failure problem may not find an appropriate failure point on the first attempt. To address these cases, we proceed by restarting the solver from a feasible point, and if that fails, we simply take a point which satisfies the line-limit constraint. The failure point methodology is outlined in [Algorithm SM2.4](#).

Algorithm SM2.3 Compute Equilibrium Point (with load shed for feasibility)

Require: Network topology \mathcal{N} , dispatch data \mathcal{D} , and dynamics parameters \mathcal{P}

```

Attempt to solve unconditional NLP for  $\hat{x}$ 
while unconditional NLP is infeasible do
     $\mathcal{I} \leftarrow i$  such that  $V_i < 0.8$  or  $V_i > 1.2$  (non-supportable bus voltage)
    Shed load at buses  $i \in \mathcal{I}$ 
    Remove lines connected to each bus in  $\mathcal{I}$ 
    Attempt to solve unconditional NLP for  $\hat{x}$ 
end while
 $\bar{x} \leftarrow \hat{x}$ 
return  $\bar{x}$ 

```

Algorithm SM2.4 Compute Failure Point

Require: Network topology \mathcal{N} , dispatch data \mathcal{D} , and dynamics parameters \mathcal{P} , line l

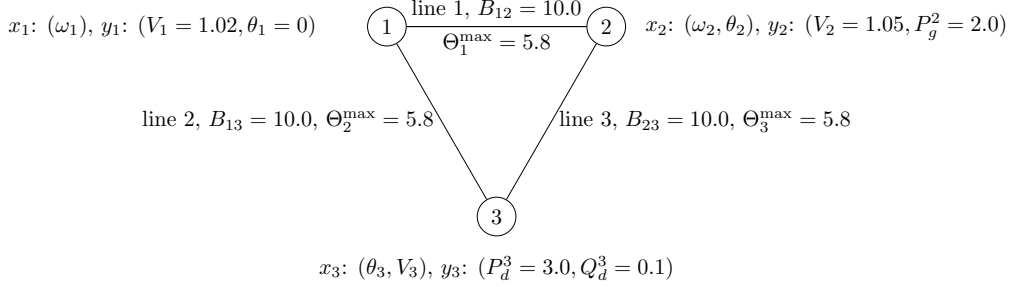
```

Attempt to solve unconditional NLP for  $\hat{x}$ 
if unconditional NLP is infeasible then
    Compute a feasible failure point  $x_f$  such that  $\Theta_l(x_f) = \Theta_l^{\max}$ 
    Attempt to solve relaxed unconditional NLP (with  $\Theta_l(x) \geq \Theta_l^{\max}$ ) for  $\hat{x}$  warm-started at  $x_f$ 
    if Relaxed unconditional NLP is infeasible then
        Solve for feasible failure point  $x_f$  such that  $\Theta_l(x_f) = \Theta_l^{\max}$ 
         $x^* \leftarrow x_f$ 
    else
         $x^* \leftarrow \hat{x}$ 
    end if
end if
return  $x^*$ 

```

SM2.3. 3-bus detailed system. The below model describes the 3bus system used to generate the energy surface contour plots and is largely based on the model in [\[SM7\]](#). Bus 1 is a generator (taken to be the slack/reference and hence its voltage angle is fixed to zero), bus 2 is a generator,

and bus 3 is a load. The component of the state space x associated with bus 1 is only ω_1 ; V_1 , θ_1 , and $P_1^g := P_3^d - P_2^g$ are fixed components of y . The components of the state space x associated with bus 2 are ω_2, θ_2 ; V_2 and P_2^g are fixed components of y . The components of the state space x associated with bus 3 are V_3 and θ_3 ; P_3^d and Q_3^d are fixed components of y . Furthermore, each line is assumed to have equal susceptance (10.0) and line limit (5.8).



SM3. Additional experiments. We present additional numerical results for failure path experiments, unconditional failure rate experiments, equilibration experiments, and cascade simulation experiments.

SM3.1. Failure path experiments. In this section, we present supplementary experiments for failure path experiments corresponding to the 118-bus system with $N\text{-}1$ secure line limits. Note that in panels (b)–(c) of Figure SM3.1, line 133 is the lowest $\Delta\mathcal{H}$ line that exhibits an additional line failure along the most likely failure path; it is a corner case in the system. For line 133's pathway, the additional failure corresponds to line 134, which has the lowest rating in the entire network. Further, the low rating assigned to line 134 is a numerical artifact of the $N\text{-}1$ procedure (Algorithm SM2.2). When setting line limits, the $N\text{-}1$ algorithm ignores “islanding” contingencies, and disconnection of line 133 automatically separates line 134 from the rest of the network; Algorithm SM2.2 did not adjust line 134's rating based on possible contingencies associated with line 133. However, increasing line 134's rating by just 6.5% would prevent pathway failure.

We also note that in panel (c), line 58's failure pathway is not shown. This line has a very large energy difference ($\Delta\mathcal{H} = 32.7$) and is associated with 127 additional line failures. We treat it as an outlier and do not plot this point.

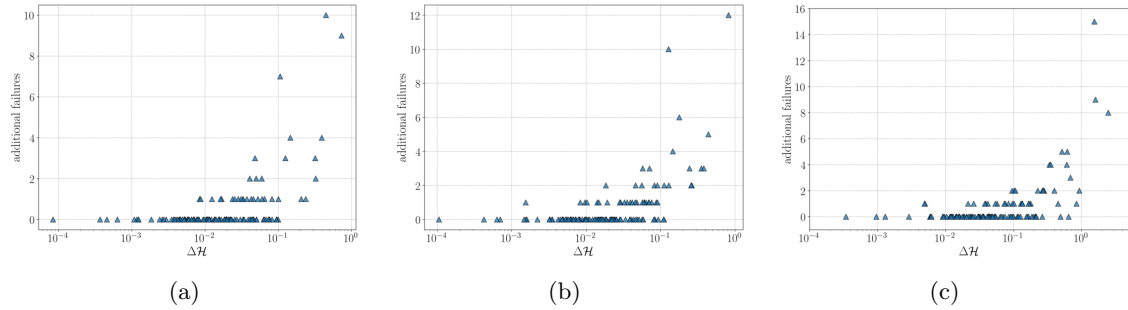


Fig. SM3.1: Study of approximate minimum energy failure path displaying number of unintended failures along the pathway from x^* to \bar{x} for a particular line in the 118-bus system. (a) $N\text{-}1$ line limits. (b) $N\text{-}1$ line limits uniformly increased by 10%. (c) $N\text{-}1$ line limits uniformly increased by 100%.

SM3.2. Unconditional failure rate experiments. In this section, we present supplementary experiments for simulation experiments corresponding to the unconditional line failure rate.

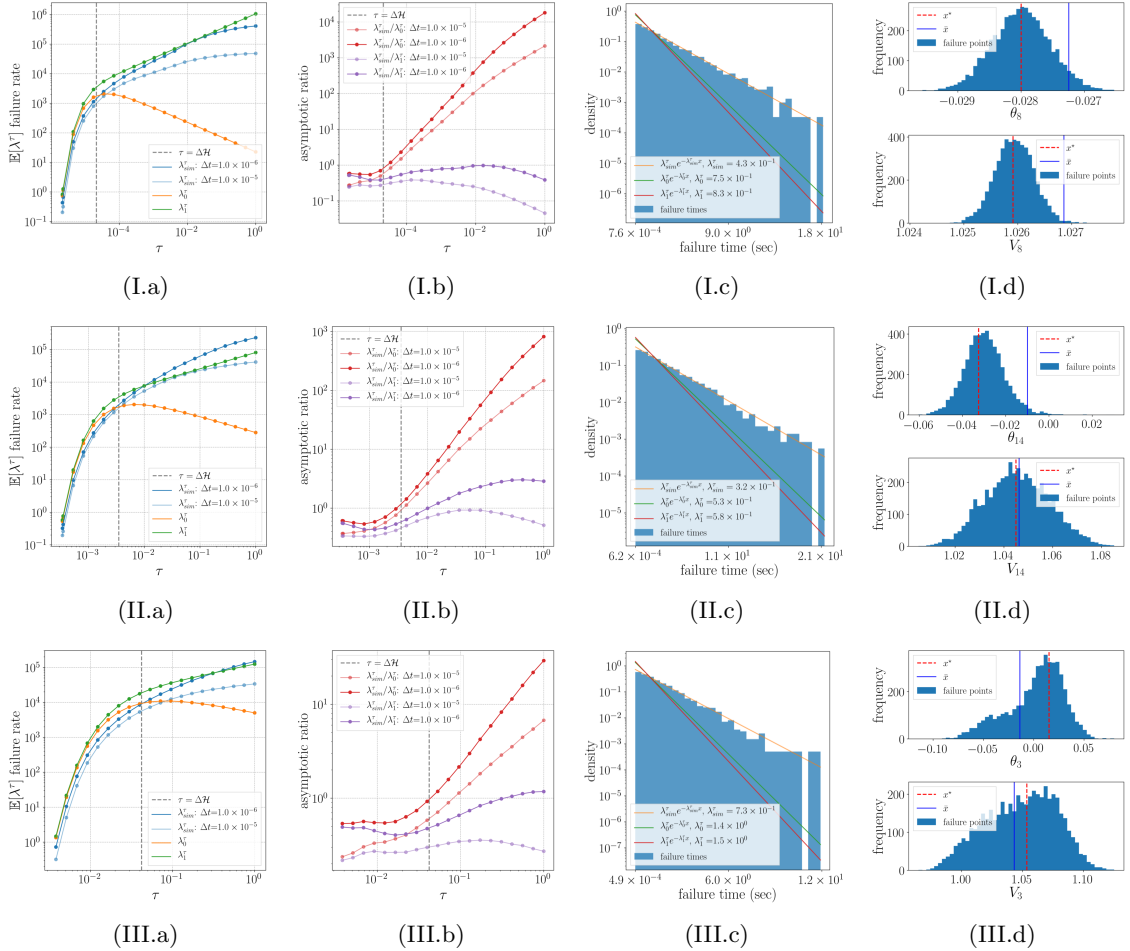


Fig. SM3.2: Unconditional line failure diagnostics for load-load lines: line 10 (I), line 20 (II), and line 4 (III). (a) Failure rate comparison across temperature. (b) Asymptotic ratio across temperature. (c) (Scaled) histogram of unconditional failure times at lowest temperature tested. (d) Histogram of x_i^* where i corresponds to the bus index of (one of) the line's connecting buses; shown at lowest temperature tested.

SUPPLEMENTARY MATERIALS: SIMULATING CASCADING TRANSMISSION LINE FAILURE SM9

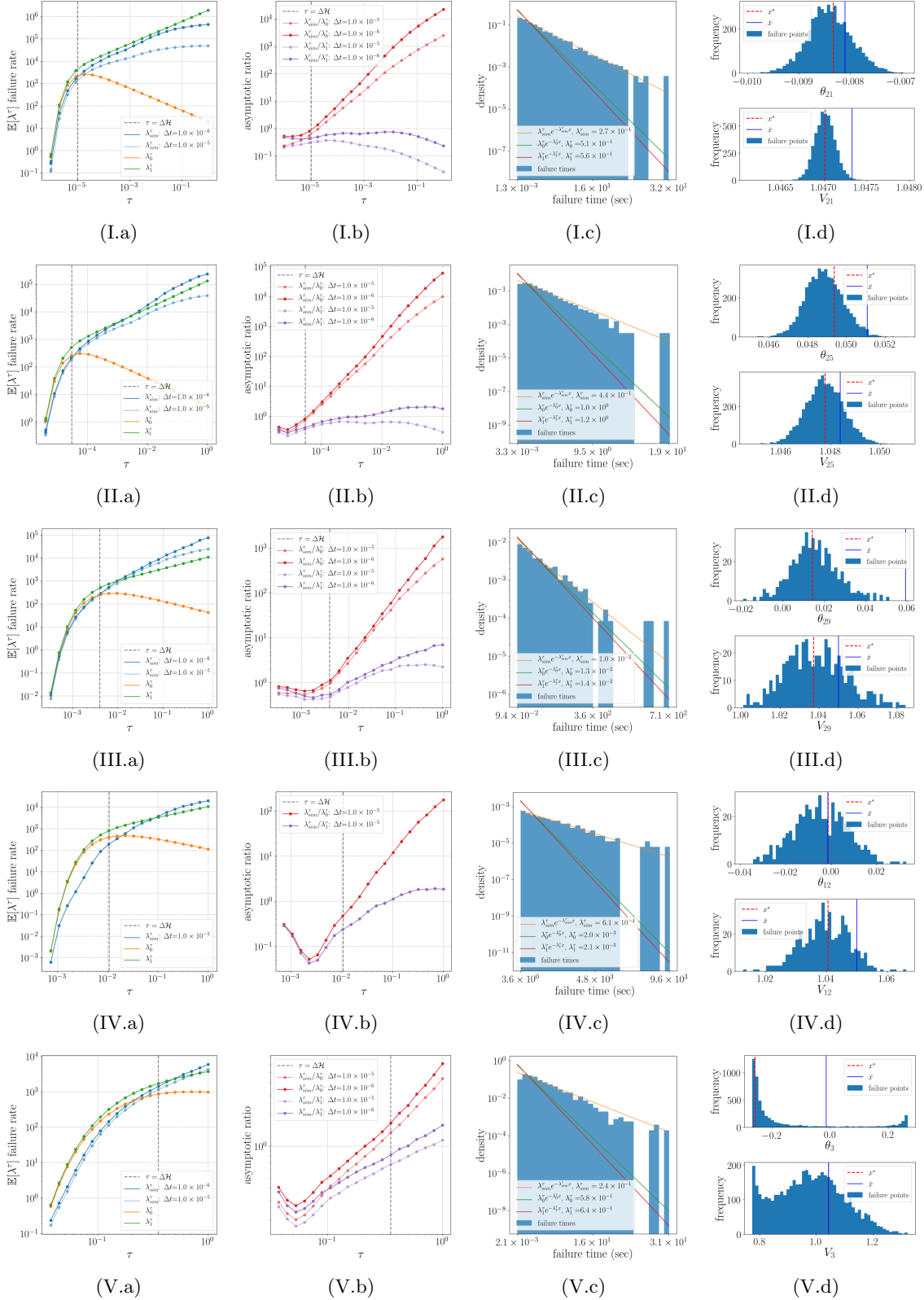
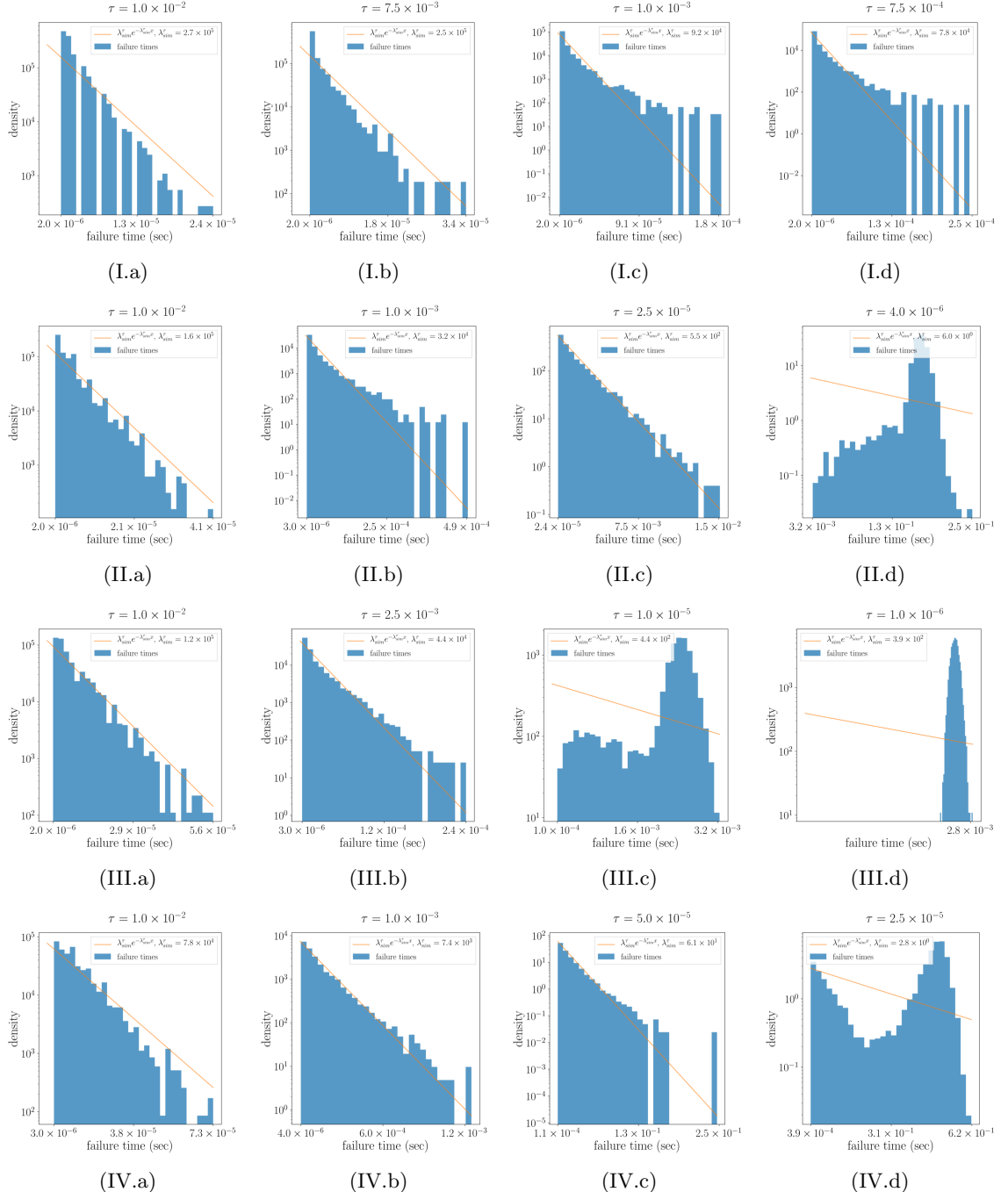


Fig. SM3.3: Unconditional line failure diagnostics for generator-load lines: line 29 (I), line 25 (II), line 37 (III), line 16, and slack-load line 2 (V). (a) Failure rate comparison across temperature. (b) Asymptotic ratio across temperature. (c) (Scaled) histogram of unconditional failure times at lowest temperature tested. (d) Histogram of x_i^* where i corresponds to the bus index of (one of) the line's connecting buses; shown at lowest temperature tested.

SM3.3. Equilibration experiments. In this section, we present supplementary experiments for our study of the dynamical equilibration between Markov states.



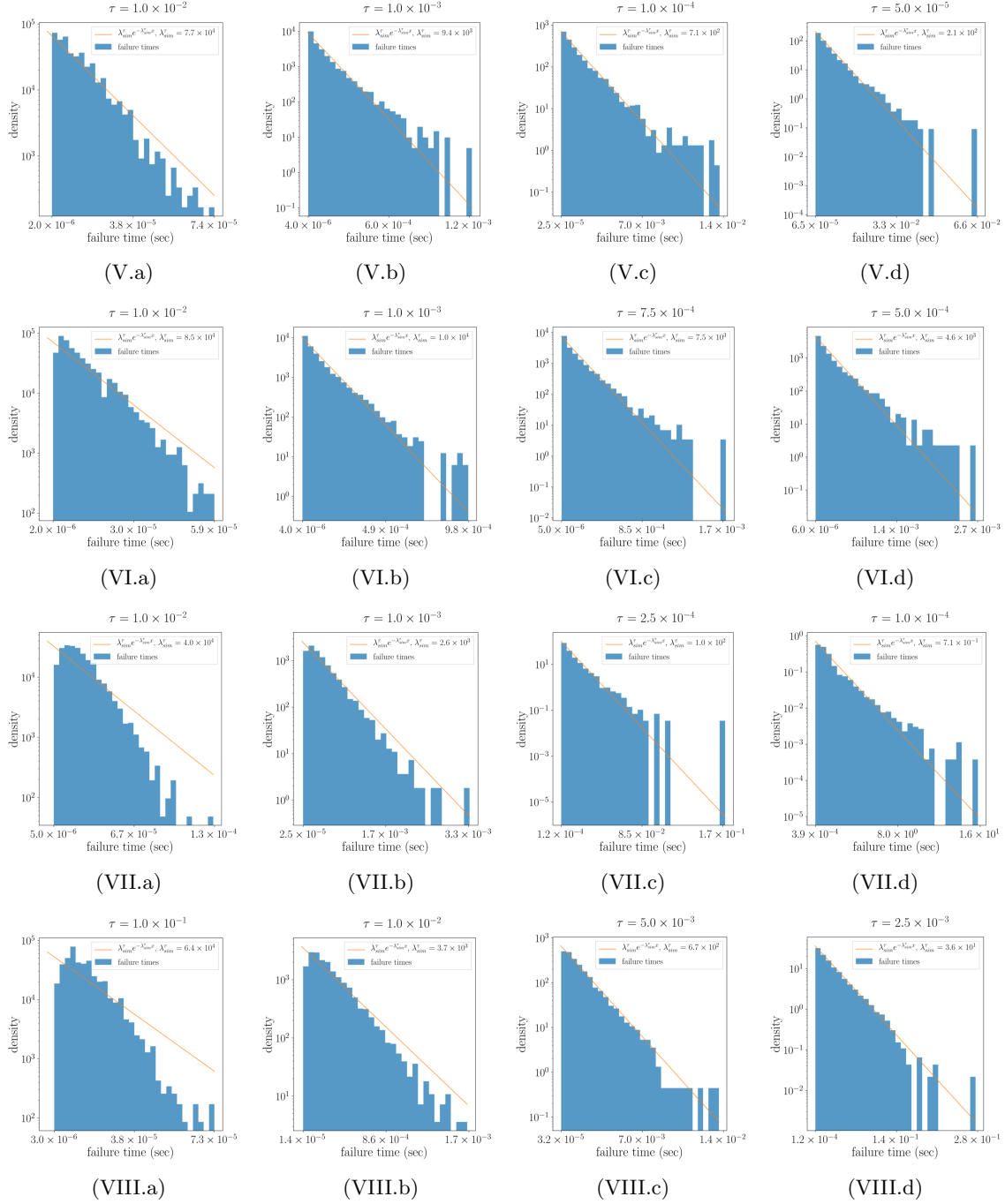


Fig. SM3.4: Equilibration study across failure depth. (I) depth 1, (II) depth 2, (III) depth 4, (IV) depth 6, (V) depth 8, (VI) depth 10, (VII) depth 12, (VIII) depth 21.

SM3.4. Cascade experiments. In this section, we present supplementary experiments for our study of temperature and network configuration on the Zipf relationships of cascade severity. We observe non-monotonicity of the SESPI with increasing temperature in two regards. First, both network configurations display oscillatory patterns of SEPSI across temperature. Second, within each Zipf plot, the failure data also demonstrate an oscillatory pattern around the power law.

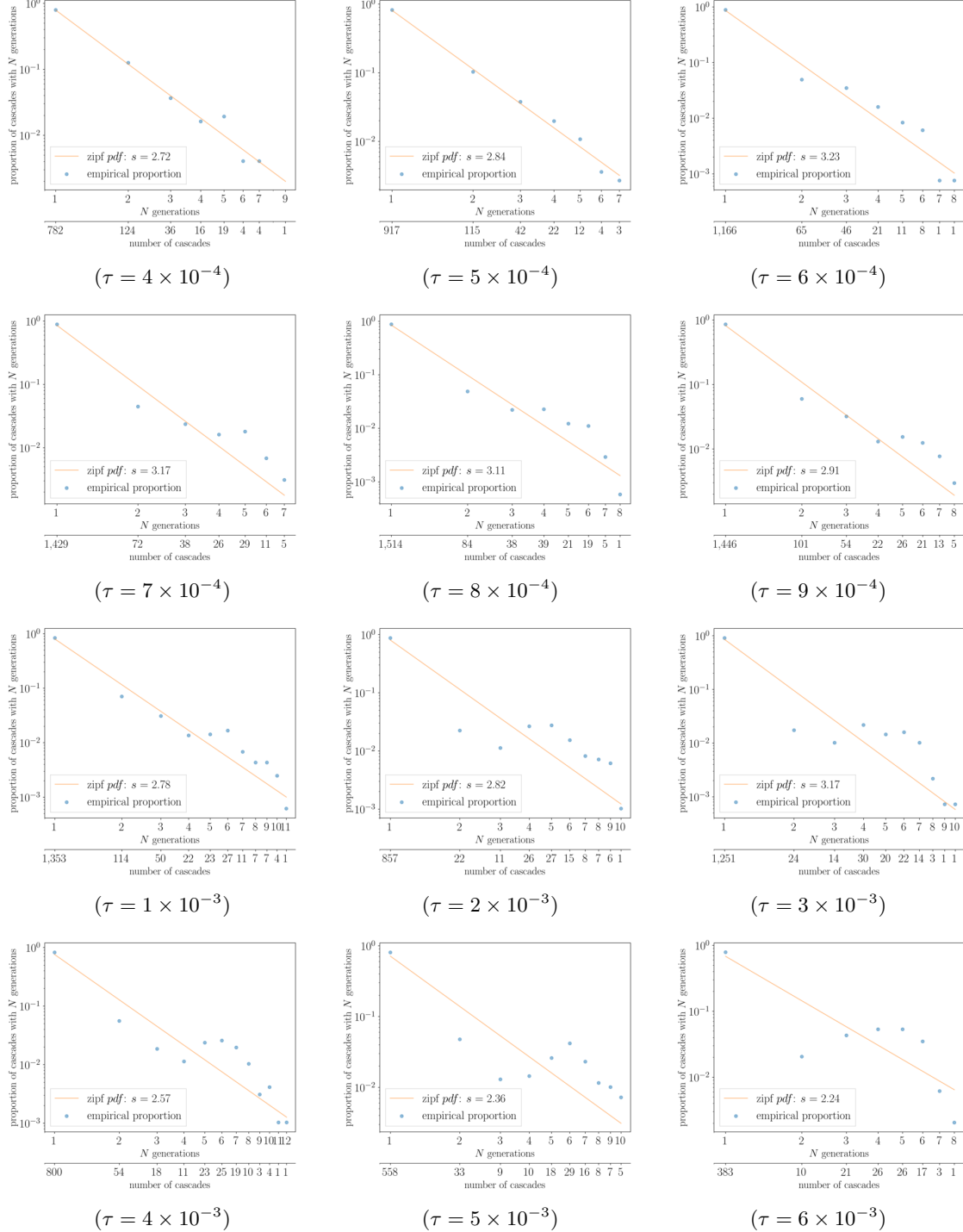
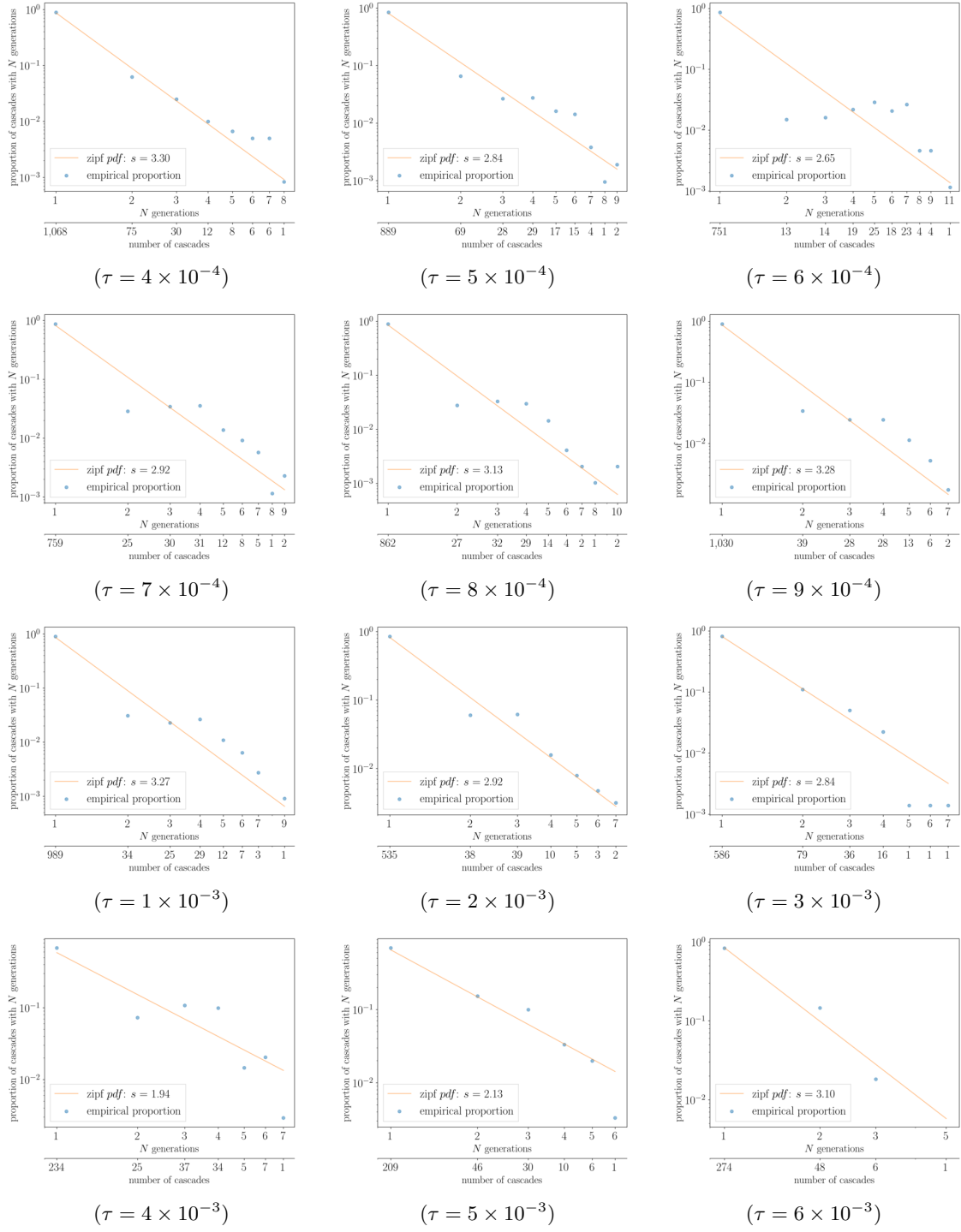


Fig. SM3.5: Zipf plots of cascades with N generations and DC line limits across temperature.

Fig. SM3.6: Zipf plots of cascades with N generations and $N-1$ line limits across temperature.

REFERENCES

- [SM1] A. R. BERGEN AND C. L. DEMARCO, *Application of singular perturbation techniques to power system transient stability analysis*, Tech. Rep. UCB/ERL-M84/7, UC Berkeley College of Engineering: Electronics Research Laboratory, February 1984.
- [SM2] C. DEMARCO AND A. BERGEN, *A security measure for random load disturbances in nonlinear power system models*, IEEE Transactions on Circuits and Systems, 34 (1987), pp. 1546–1557.
- [SM3] I. DOBSON, B. A. CARRERAS, V. E. LYNCH, AND D. E. NEWMAN, *Complex systems analysis of series of blackouts: Cascading failure, critical points, and self-organization*, Chaos: An Interdisciplinary Journal of Nonlinear Science, 17 (2007), p. 026103.
- [SM4] S. FRANK AND S. REBENNACK, *A Primer on Optimal Power Flow: Theory, Formulation, and Practical Examples*, Working Papers 2012-14, Colorado School of Mines, Division of Economics and Business, Oct. 2012.
- [SM5] N. NARASIMHAMURTHI AND M. MUSAVI, *A generalized energy function for transient stability analysis of power systems*, IEEE Transactions on Circuits and Systems, 31 (1984), pp. 637–645.
- [SM6] M. PAI, *Energy function analysis for power system stability*, (1989).
- [SM7] H. ZHENG AND C. L. DEMARCO, *A bi-stable branch model for energy-based cascading failure analysis in power systems*, North American Power Symposium 2010, (2010), pp. 1–7.
- [SM8] H. ZHENG AND C. L. DEMARCO, *A new dynamic performance model of motor stalling and fidvr for smart grid monitoring/planning*, IEEE Transactions on Smart Grid, 7 (2016), pp. 1989–1996.